Journal of
Renewable Energy Research and Applications (RERA)
Vol. 7, No 1, 2026, 139-147 DOI: 10.22044/rera.2026.17739.1544

A Hybrid Whale-Fishier Mantis Optimizer for Accurate Parameter Identification in Single-, Double-, and Triple-Diode PV Models, with a Cross-Validated Assessment of Deep-Learning Residual Correction

Ben El Haj. Marouan* and S. Ziani

Mohammed V University Rabat, Morocco.

Received Date 24 May 2026; Revised Date 15 August; Accepted Date 18 August
**Corresponding author: marouan_benelhaj@um5.ac.ma (Ben El Haj. Marouan)*

Abstract

Reliable extraction of PV module electrical parameters constitutes a critical step toward enabling fault detection and performance assessment. The strong dependence of these parameters on environmental factors, particularly solar irradiance and cell operating temperature, introduces significant nonlinearity that complicates their accurate identification. This paper proposes a hybrid metaheuristic framework, combining the Whale Optimization Algorithm (WOA) for global search with the Fishier Mantis Optimizer (FMO) for local refinement, for the parameter identification of single-, double-, and triple-diode PV models (SDM, DDM, TDM). A Bidirectional Long Short-Term Memory (BiLSTM) network is additionally investigated as a candidate residual corrector between the equivalent-circuit simulation and the measured current. Experimental validation uses current-voltage (I-V) data measured from the Solarex MSX60 module at three irradiance levels (600, 800, 1000 W/m², 25 °C). In a fair benchmark where PSO, GA, standard WOA, and two modern (post-2019) metaheuristics — the Arithmetic Optimization Algorithm (AOA) and the Slime Mould Algorithm (SMA) — are equipped with the same Latin-Hypercube initialization, opposition-based learning, and reflection-based boundary handling as the proposed method, WOA-FMO attains a physical-parameter RMSE of 3.71×10^{-2} A on all three topologies, significantly outperforming every baseline, classic and modern alike (Wilcoxon rank-sum, $p<0.01$ in all ten pairwise comparisons), at a comparable computational cost.

Keywords: *Whale Optimization Algorithm (WOA), Fishier Mantis Optimizer (FMO), deep learning, BiLSTM, multi-diode model, irradiance variation.*

1. Introduction

Solar photovoltaic technology has established itself as one of the fastest-growing renewable energy sectors worldwide, driven by declining installation costs and increasing energy demand. Accurate circuit-level modeling of PV modules is fundamental to a broad range of applications, including system sizing, output performance forecasting, fault isolation, and maximum power point tracking (MPPT) control under variable irradiance and temperature conditions. Among the available circuit representations, the single-diode model (SDM), double-diode model (DDM), and triple-diode model (TDM) stand out as the most widely adopted equivalent-circuit formulations, offering a practical trade-off between physical accuracy and computational tractability.

Each of these models involves a distinct set of unknown parameters: five for the SDM, seven for the DDM, and nine for the TDM. These parameters include the light-generated current I_{ph}, one or more diode reverse saturation currents I_{0i}, the series resistance R_s, the shunt resistance R_{sh}, and the diode ideality coefficients n_i. These parameters must be derived from experimental current-voltage (I-V) characteristics. The inverse problem inherent in this parameter extraction is characterized by non-convexity, multimodality, and a pronounced sensitivity to initial parameter estimates. Deterministic analytical techniques, including Newton-Raphson solvers coupled with the Lambert W function [1] and the iterative procedure introduced by Easwarakhanthan et al. [2], are inherently limited in their ability to handle the nonconvex nature of the parameter extraction problem and are susceptible to premature convergence at local optima in the presence of measurement uncertainty.

Nature-inspired metaheuristic methods have attracted growing research interest over the last two decades as viable alternatives for global optimization in PV parameter identification. Representative techniques, including Particle Swarm Optimization (PSO) [3], Genetic Algorithms (GA) [4], and the Whale Optimization Algorithm (WOA) [5], have demonstrated competitive performance across various benchmark test cases [6], [7]. However, these approaches share several recurring shortcomings: slower convergence in high-dimensional search spaces (as encountered in DDM and TDM problems), uneven fitting accuracy along distinct segments of the I-V characteristic and limited robustness to measurement artifacts and modeling uncertainties.

The integration of metaheuristic optimization with physics-aware machine learning has recently emerged as a promising direction for addressing the inherent limitations of standalone population-based algorithms. Although global search methods provide broad exploration capabilities in the early optimization stages, their convergence behavior typically degrades in later iterations. Deep learning architectures, particularly Bidirectional Long Short-Term Memory (BiLSTM) networks [8], [9], offer strong capacity to model complex, nonlinear residual patterns. Whether such a corrector meaningfully improves parameter identification, however, can only be established once it is evaluated on data it has not seen during training and hyperparameter selection. This paper therefore investigates the BiLSTM stage under a leave-one-irradiance-out cross-validation protocol rather than assuming a priori that it helps.

The methodology operates in two sequential stages under varying irradiance conditions. In the first stage, the Whale Optimization Algorithm (WOA) and the Fishier Mantis Optimizer (FMO) [10] are combined to provide, respectively, broad global exploration and targeted local exploitation of the parameter space. In the second stage, a BiLSTM network is trained and rigorously cross-validated as a candidate residual corrector on the simulated current.

The main contributions of this work are as follows:

- A constrained hybrid optimization framework combining WOA and FMO is formulated for PV parameter extraction, explicitly accounting for irradiance-dependent photocurrent variation and enforcing physically meaningful bounds on all estimated parameters.
- Multiple algorithmic improvements are incorporated to enhance search performance: a population seeding strategy based on Latin Hypercube Sampling augmented with Opposition-Based Learning (LHS-OBL), a reflection-based boundary management scheme, and an adaptive elitism mechanism. Critically, these same enhancements are also applied to the PSO, GA, standard WOA, AOA, and SMA baselines used for comparison, isolating the benefit of the WOA-FMO hybridization itself from that of the shared engineering add-ons.
- A candidate BiLSTM-based residual-correction module is evaluated under leave-one-irradiance-out cross-validation, together with an input-feature ablation study. We transparently report that this module does not improve generalization accuracy on the present dataset and discuss the implications (Section 4.3).
- A rigorous statistical validation using Wilcoxon rank-sum and ANOVA tests over 10 independent runs confirms the superiority and robustness of the proposed WOA-FMO optimizer compared to fairly-equipped PSO, GA, standard WOA, AOA, and SMA baselines ($p<0.01$ in all ten pairwise comparisons), along with a systematic comparison of CPU execution time.

The remainder of the paper is organized as follows. Section 2 reviews the state of the art in PV module modeling. Section 3 details the proposed methodology, including the cross-validation protocol and the fair-benchmark procedure. Section 4 presents the results and the study's limitations. Section 5 concludes and outlines future work.

2. State of the art

Photovoltaic modules can be characterized by various equivalent circuit models, typically differentiated by their diode topologies. Three widely recognized models are examined here: the single-diode model (SDM) [11], the double-diode model (DDM) [12], and the triple-diode model (TDM) [13].

2.1. Single-diode model (SDM)

For a PV module comprising N_s series-connected identical silicon cells operating at a junction temperature **T** (in K), the SDM current **I** as a function of terminal voltage **V** is given implicitly by equation (1):

$$\mathbf{I} = \mathbf{I_{ph}} - \mathbf{I}_0\left(\mathbf{e}^{\frac{(\mathbf{V}+\mathbf{IR_s})}{\mathbf{nV_tN_s}}} - 1\right) - \frac{\mathbf{V}+\mathbf{IR_s}}{\mathbf{R_{sh}}} \qquad (1)$$

where $\mathbf{V_t}$ = kB·T/q denotes the thermal voltage of one cell, **kB** is the Boltzmann constant (1.380649×10^{-23} J/K), **q** is the elementary charge (1.602×10^{-19} C), $\mathbf{I_{ph}}$ denotes the photogenerated current, I0 is the diode saturation current, $\mathbf{R_s}$ is the series resistance, $\mathbf{R_{sh}}$ is the shunt resistance, and n denotes the ideality factor.

2.2. Double-diode model (DDM)

The DDM incorporates a second diode to explicitly model recombination losses occurring within the space-charge region (Equation (2)):

$$\mathbf{I} = \mathbf{I_{ph}} - \mathbf{I}_{01}\left(\mathbf{e}^{\frac{(\mathbf{V}+\mathbf{IR_s})}{\mathbf{n_1 V_t N_s}}} - 1\right) - \mathbf{I}_{02}\left(\mathbf{e}^{\frac{(\mathbf{V}+\mathbf{IR_s})}{\mathbf{n_2 V_t N_s}}} - 1\right) - \frac{\mathbf{V}+\mathbf{IR_s}}{\mathbf{R_{sh}}} \quad (2)$$

where I_{01} and I_{02} are the saturation currents of the two diodes, and n_1 and n_2 are their ideality factors. The other symbols are as defined in equation (1).

2.3. Triple-diode model (TDM)

The TDM extends this by including a third diode, thereby accommodating recombination losses at lower voltages and leakage currents at the cell perimeter (Equation (3)):

$$\mathbf{I} = \mathbf{I_{ph}} - \sum_{\mathbf{i}=1}^{3}\mathbf{I}_{0\mathbf{i}}\left(\mathbf{e}^{\frac{(\mathbf{V}+\mathbf{IR_s})}{\mathbf{n_i V_t N_s}}} - 1\right) - \frac{\mathbf{V}+\mathbf{IR_s}}{\mathbf{R_{sh}}} \quad (3)$$

given that equations (2) and (3) lack analytical solutions, a damped Newton-Raphson scheme is employed, initialized using the Lambert-W solution of an equivalent SDM with effective saturation current $\sum_i I_{0i}$.

2.4. Optimization problem formulation

The process of parameter extraction is formulated as an optimization problem, specifically the minimization of the Root-Mean-Square Error (RMSE) between measured and simulated currents across all experimental data points and irradiance conditions (Equation (4)):

$$\mathbf{RMSE}(\theta) = \sqrt{\frac{1}{\mathbf{N}}\sum_{\mathbf{k}}\sum_{\mathbf{j}}\left[(\mathbf{I_{meas,k,j}} - (\mathbf{I_{sim}}\left(\mathbf{V_{k,j}}, \theta, \mathbf{G_k}\right)\right]^2} \quad (4)$$

where N is the total number of measurement points across the K irradiance datasets, and θ is the parameter vector ($|\theta| \in \{5, 7, 9\}$ for SDM, DDM, TDM, respectively).

3. Methodology

The proposed methodology employs a two-stage hybrid architecture: first, metaheuristic optimization using the WOA-FMO algorithm; and second, a residual-error correction stage with a BiLSTM network, which determines whether it is retained in the final pipeline.

3.1. Hybrid WOA-FMO algorithm

The algorithm developed for this study integrates the Whale Optimization Algorithm (WOA) for its global exploration capabilities with the Fishier Mantis Optimizer (FMO) to facilitate the local refinement of promising candidate solutions.

Several engineering enhancements are incorporated into the foundational scheme: Latin Hypercube Sampling for a stratified initialization of the population; Opposition-Based Learning, which augments population diversity by evaluating each candidate xi alongside its opposite lb+ub−xi and retaining whichever yields the lower RMSE; reflection-based bound handling, chosen over simple clipping, to avert parameter accumulation at boundaries; and elitism preservation, where the global best solution consistently replaces the current worst solution in each generation.

The population size is defined as P=max(80,10×dim, ensuring that the higher-dimensional TDM search (dim=9) is allocated a sufficiently rich population (P=90), comparable to those used for the SDM (dim=5, P=80) and DDM (dim=7, P=80). This strategy is adopted to prevent the use of a fixed population size from leading to insufficient sampling of the 9-dimensional TDM search space relative to the lower-dimensional models.

3.2. BiLSTM residual corrector and cross-validation protocol

The three irradiance curves (600, 800, 1000 W/m², all at 25 °C) are used in a leave-one-irradiance-out cross-validation scheme. For each of the three folds, one curve is held out entirely as the test set; of the remaining two curves, one is used to train the BiLSTM network and the other is used exclusively to select the fusion weight λ_{DL} by grid search (0.025 resolution over [0,1]) and for early-stopping monitoring. Feature normalization statistics (mean and standard deviation of V, G, I_{sim}, and I_{meas}) are computed on the training curve only and applied unchanged to the validation and test curves, avoiding all forms of leakage. The RMSE reported for the BiLSTM+physics fusion is the mean over the three held-out test folds.

The BiLSTM network consists of one bidirectional LSTM layer with 48 hidden units, a dropout layer (rate 0.15), a fully connected layer (24 units) with ReLU activation, and a linear output layer [14]. The candidate input to the network is a sequence of features per operating point: the terminal voltage V, the irradiance level G, and the physics-model-simulated current I_{sim}; an ablation configuration using only (V, G) is also evaluated. The network is trained for up to 150 epochs using the Adam optimizer [15] with an initial learning rate of 5×10^{-3}, reduced by a factor of 0.5 every 50 epochs, L2 weight regularization ($\lambda=1\times10^{-4}$), and a mini-batch size of 1.

The fused current output, when the BiLSTM stage is retained, is expressed by equation 5:

$$\mathbf{I_{final}} = \boldsymbol{\lambda}_{\mathbf{DL}}.\mathbf{I_{sim}} + \left(1-\boldsymbol{\lambda}_{\mathbf{DL}}\right).\mathbf{I_{DL}} \qquad (5)$$

3.3. Experimental setup

The proposed methodology was validated on the Solarex MSX60 photovoltaic module [16] using experimental I-V curves acquired at three irradiance levels: 600, 800, and 1000 W/m², all measured at a cell temperature of 25°C. The module is composed of N_s=36 silicon cells in series, with rated values V_{oc}=21.1 V, I_{sc}=3.8 A, V_{mpp}=17.1 V, and I_{mpp}=3.5 A.

The algorithm's hyperparameters were configured as follows: a base population size P=80 (scaled with dimensionality per Section 3.1), a total of G=300 generations, FMO coefficients $\beta_1=\beta_2=1.5$, an initial elite fraction τ=30% (linearly decreasing to 1% over generations), and a spiral shape parameter b=1. To facilitate robust statistical analysis, the optimization process was executed across 10 independent runs. CPU execution time was recorded for each run.

3.4. Benchmark protocol against classic and modern metaheuristics

Each competing algorithm—PSO, GA, WOA, and two modern (post-2019) metaheuristics, the Arithmetic Optimization Algorithm (AOA) [17] and the Slime Mould Algorithm (SMA) [18]—is run in two variants: a vanilla variant, implementing the textbook algorithm with uniform random initialization and simple clipping at the bounds; and an enhanced variant, equipped with identical LHS+OBL initialization and reflection-based boundary handling used by WOA-FMO. All six algorithms are evaluated on the same SDM problem, with the same population size, number of generations, and 10 independent runs, and their wall-clock CPU time is recorded for each run.

4. Results and discussion

This section presents the convergence behavior and physical parameter identification, the residual analysis, the honest cross-validated assessment of the BiLSTM residual corrector and its input-feature ablation, the fair comparison with PSO, GA, and standard WOA, and a discussion of the study's limitations.

Figure 1 plots the mean RMSE (± standard deviation) over 10 independent runs across 300 generations, for the physical WOA-FMO parameter identification (i.e., before any BiLSTM correction is considered). The three diode models exhibit similar asymptotic convergence behaviour, all stabilising in the narrow range [3.7086, 3.7095]$\times10^{-2}$ A (Table 2). Once the population size is scaled with problem dimensionality, the residual gap between the SDM, DDM and TDM mean RMSE values ($\leq9\times10^{-6}$ A, table 2) falls within one standard deviation of the run-to-run variability, indicating that the observed difference is not practically meaningful, though it was not subjected to a formal significance test.

Table 1 reports the physical parameters identified by WOA-FMO alone, together with the corresponding fit-quality metrics.

The simulated I-V and P-V curves are compared with the experimental measurements in figures 2, 3, and 4 for SDM, DDM, and TDM, respectively (physical model, no BiLSTM correction applied). All three models reproduce the measurements with excellent visual agreement at the three irradiance levels.

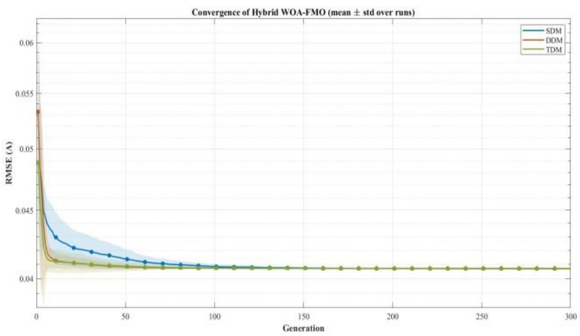

Figure 1. Convergence of the hybrid WOA-FMO algorithm (mean RMSE over 10 runs), physical parameters only.

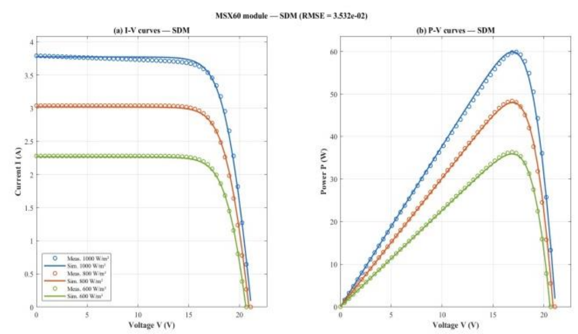

Figure 2. Measured vs. simulated I-V and P-V curves for the SDM (physical parameters, WOA-FMO only).

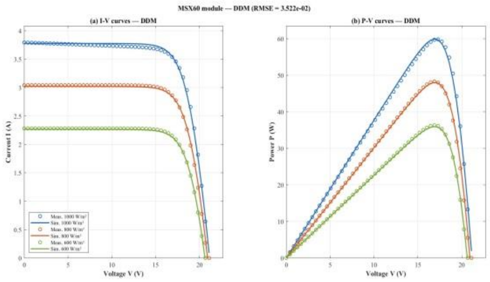

Figure 3. Measured vs. simulated I-V and P-V curves for the DDM (physical parameters, WOA-FMO only).

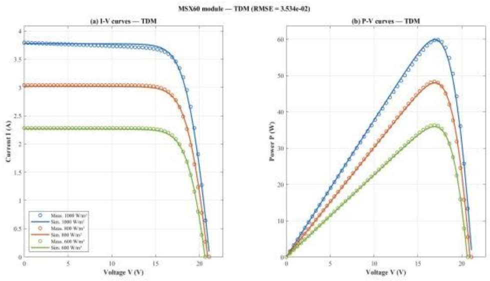

Figure 4. Measured vs. simulated I-V and P-V curves for the TDM (physical parameters, WOA-FMO only).

Table 1. Physical parameters and fit-quality metrics identified by WOA-FMO alone (best of 10 runs), before any BiLSTM correction is applied.

Parameter	SDM	DDM	TDM
I_{ph} (A)	3.77681	3.77764	3.77748
I_{01} (A)	5.177e-9	4.443e-9	4.485e-9
I_{02} (A)	–	4.999e-8	4.971e-9
I_{03} (A)	–	–	1.711e-9
R_s (Ω)	0.3791	0.3826	0.3808
R_{sh} (Ω)	3499.9	3999.9	2996.3
n_1	1.1211	1.1129	1.1139
n_2	–	1.7896	1.4230
n_3	–	–	1.9400
RMSE (A)	3.7086e-2	3.7067e-2	3.7090e-2
MAE (A)	2.7474e-2	2.7258e-2	2.7498e-2
MBE (A)	+3.837e-3	+2.995e-3	+3.769e-3
R^2	0.998179	0.998181	0.998179
NRMSE (%)	1.344	1.344	1.345

Table 2. Statistical RMSE performance of WOA-FMO optimization over 10 independent runs (physical parameters only).

Statistic	SDM	DDM	TDM
min (A)	3.7086e-2	3.7067e-2	3.7090e-2
max (A)	3.7102e-2	3.7100e-2	3.7117e-2
mean (A)	3.7090e-2	3.7086e-2	3.7095e-2
std (A)	5.80e-6	9.27e-6	8.73e-6
median (A)	3.7087e-2	3.7088e-2	3.7091e-2

The narrow interquartile ranges (Figure 5) confirm the high reproducibility of the proposed optimizer across independent runs for all three topologies, including the TDM once its population is scaled to its higher dimensionality.

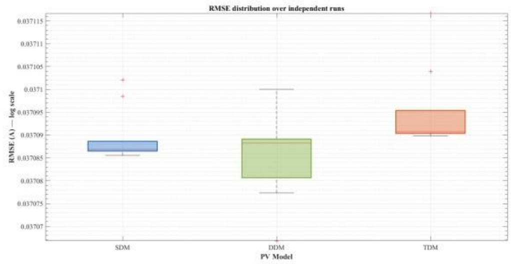

Figure 5. RMSE distribution over 10 independent runs (physical parameters, log scale).

All three models show a comparable residual pattern: a small positive bias in the constant-current region and a larger, structured excursion near the knee and open-circuit voltage — the typical signature of an equivalent-circuit model fitting a real module with several I-V curves fitted jointly (Figure 6). The near-identical residual statistics across SDM, DDM, and TDM ($\mu \approx 3.0$–3.8×10^{-3} A, $\sigma \approx 3.7\times10^{-2}$ A for all three) mirror the near-identical RMSE values in table 1 and confirm that adding diodes beyond the SDM does not measurably change the fit quality on this dataset once the optimizer is given comparable search resources.

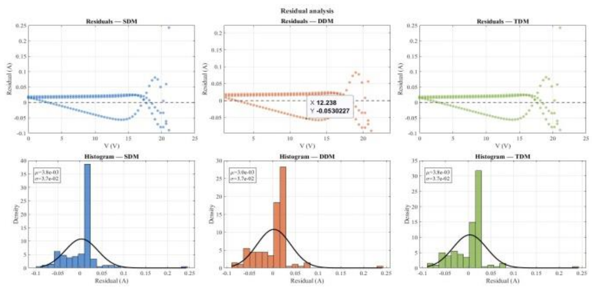

Figure 6. Residual analysis (Imeas − Isim) vs. voltage (top) and density with Gaussian fit (bottom), physical model only.

Table 3 reports the leave-one-irradiance-out cross-validated RMSE of the BiLSTM+physics fusion, i.e. the RMSE measured on a held-out irradiance curve that was used neither to train the network nor to select λ_{DL}.
The cross-validated grid search selects λ_{DL}=1 in every one of the three folds for all three diode topologies. Since I_{final} is expressed by equation 5, λ_{DL}=1 means the BiLSTM output is entirely discarded, and the fused prediction reduces to the physical-model output alone (Figure 7). In other

words, once evaluated on a held-out irradiance curve, the BiLSTM correction never improves on the physical model.

Table 3. Leave-one-irradiance-out cross-validated RMSE of the BiLSTM+physics fusion.

Model	Mean CV test RMSE (A)	Std (A)	Selected λ_{DL} (all folds)
SDM	3.5324e-2	1.3483e-2	1.000
DDM	3.5218e-2	1.3809e-2	1.000
TDM	3.5339e-2	1.3440e-2	1.000

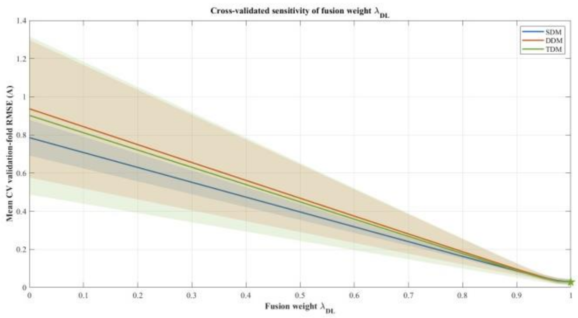

Figure 7. Cross-validated sensitivity of the fusion weight on the validation fold as a function of λ_{DL}, for the three diode topologies. The minimum is reached at λ_{DL}=1 (physical model only, starred) for every model.

An ablation study compares the BiLSTM trained with (V, G, I_{sim}) against a variant trained with (V, G) only, under the same leave-one-irradiance-out protocol (Table 4).

Table 4. Ablation study: BiLSTM test RMSE with vs. withou I_{sim} as an input feature (leave-one-irradiance-out CV).

Model	With I_{sim} (A)	Without I_{sim} (A)	Δ (without − with)
SDM	3.5324e-2	3.5324e-2	0.0000e+0
DDM	3.5218e-2	3.5218e-2	0.0000e+0
TDM	3.5339e-2	3.5339e-2	0.0000e+0

The two configurations yield identical honest RMSE for every model. This is a direct algebraic consequence of the λ_{DL}=1 finding above: because the fused prediction discards the BiLSTM output in every fold regardless of its input features, whether I_{sim} is included cannot change the reported RMSE.

Table 5 compares WOA-FMO against PSO, GA, standard WOA, and two modern (post-2019) metaheuristics — the Arithmetic Optimization Algorithm (AOA) [17] and the Slime Mould Algorithm (SMA) [18], both already used in the multi-diode PV parameter-extraction literature — on the SDM. Each baseline is run in both a vanilla configuration (textbook algorithm, uniform random initialization, simple clipping) and an enhanced configuration (same LHS+OBL initialization and reflection-based boundary handling as WOA-FMO), over 10 independent runs, together with mean CPU execution time per run.

Table 5. Fair benchmark on the SDM: vanilla vs. enhanced PSO/GA/WOA/AOA/SMA against the proposed WOA-FMO (10 runs each).

Algorithm	Mean RMSE (A)	Std (A)	Mean time (s)
PSO (vanilla)	3.8047e-2	1.911e-3	17.66
PSO (enhanced)	3.7162e-2	1.053e-4	11.25
GA (vanilla)	3.9355e-2	1.141e-3	11.73
GA (enhanced)	3.9550e-2	9.699e-4	11.31
WOA (vanilla)	3.9905e-2	2.102e-3	13.98
WOA (enhanced)	3.7654e-2	4.417e-4	18.35
AOA (vanilla) [17]	5.0877e-2	1.293e-2	18.45
AOA (enhanced)	3.9821e-2	2.038e-3	17.94
SMA (vanilla) [18]	3.8060e-2	7.846e-4	17.03
SMA (enhanced)	3.7724e-2	5.462e-4	17.40
WOA-FMO (proposed)	3.7071e-2	2.835e-5	22.14

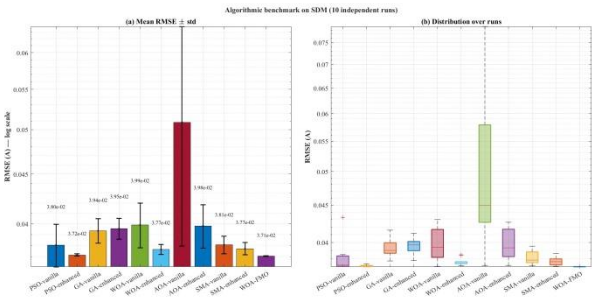

Figure 8. Algorithmic benchmark on the SDM (10 independent runs): (a) mean RMSE ± std (log scale), (b) RMSE distribution per algorithm.

Three observations follow from table 5 and figure 8. First, the LHS+OBL+reflection enhancements measurably improve PSO, WOA, and, most dramatically, AOA (mean RMSE drops from 5.09×10^{-2} A to 3.98×10^{-2} A, and std from 1.29×10^{-2} A to 2.04×10^{-3} A — nearly an order of magnitude), confirming that part of any such algorithm's reported performance is attributable to initialization/boundary-handling engineering rather than the algorithm's search mechanism alone. The enhancements leave GA essentially unchanged and only modestly improve SMA, which is already comparatively stable in its vanilla form. Second, the modern algorithms do not automatically outperform the classic ones on this problem: vanilla AOA is in fact the worst-performing and least reliable method in the entire benchmark (mean 5.09×10^{-2} A, std 1.29×10^{-2} A — more than an order of magnitude less consistent than every other vanilla baseline), consistent with reports in the wider optimization literature that AOA is prone to premature convergence without careful initialization; SMA performs competitively with, but does not exceed, the enhanced classic baselines. Third, and most importantly, WOA-FMO significantly outperforms every method in the comparison, classic and modern alike, both in mean RMSE and — by one to two orders of magnitude — in run-to-run standard deviation (2.8×10^{-5} A), underscoring that the hybridization contributes a genuine benefit beyond both the shared engineering add-ons and the more recent search mechanisms of AOA/SMA. The computational cost of WOA-FMO (mean 22.1 s per run in this session) remains in the same range as every baseline (11.3–18.5 s), not an order of magnitude larger.

A one-way ANOVA across the eleven groups strongly rejects the null hypothesis of equal RMSE ($p=1.55\times10^{-10}$). Pairwise Wilcoxon rank-sum tests (Table 6) confirm that WOA-FMO is significantly better than every other method — including both modern algorithms, in both their vanilla and enhanced forms — in every pairwise comparison [19], [20].

A dedicated CPU-timing table for the SDM/DDM/TDM WOA-FMO optimizations themselves (as opposed to the SDM-only cross-algorithm benchmark above) is given in table 7.

Table 6. Pairwise Wilcoxon rank-sum tests, WOA-FMO vs. each baseline (n=10 runs each). ANOVA across all 11 groups: $p=1.55\times10^{-10}$.

Comparison (vs. WOA-FMO)	p-value
PSO (vanilla)	1.706e-3
PSO (enhanced)	5.795e-3
GA (vanilla)	1.827e-4
GA (enhanced)	1.827e-4
WOA (vanilla)	3.298e-4
WOA (enhanced)	1.827e-4
AOA (vanilla)	1.827e-4
AOA (enhanced)	1.827e-4
SMA (vanilla)	1.827e-4
SMA (enhanced)	2.461e-4

Table 7. Mean CPU execution time of WOA-FMO per independent run, at the population/generation budget used for the headline results (10 runs each).

Model	dim	Mean time (s)	Std (s)
SDM	5	23.16	4.43
DDM	7	33.74	1.92
TDM	9	49.58	15.89

The fused current defined in (5) combines the physical-model prediction with a neural-network correction. Consequently, the output is primarily optimized for predictive accuracy and is not explicitly constrained to satisfy all electrical relationships imposed by the equivalent-circuit formulation. Therefore, for applications requiring strict circuit consistency, the physical parameters identified by WOA-FMO should be preferred over the unconstrained fused current. In the present study, however, this distinction has no impact on the reported results, since the cross-validation analysis yields $\lambda_{DL}=1$ for all validation folds and considered neural-network architectures. The final model therefore relies exclusively on the WOA-FMO physical solution, without an effective contribution from the neural-network correction.

A further limitation is that all validation data were acquired under uniform irradiance in controlled laboratory conditions; partial-shading scenarios, which are common in field deployments and introduce multiple current peaks and local maxima not represented in the present dataset, were not evaluated. Assessing WOA-FMO under partial-shading I-V profiles is left for future work.

The comparison between the double-diode model (DDM) and triple-diode model (TDM) also highlights the effect of model complexity on parameter identifiability. The introduction of a third diode does not provide a measurable RMSE improvement for the investigated dataset: the TDM's mean RMSE (3.7095×10^{-2} A, table 2) is in fact marginally higher than that of the DDM (3.7086×10^{-2} A), a gap of approximately 9×10^{-6} A that falls within one run-to-run standard deviation of either model ($\sigma = 8.73\times10^{-6}$ A and 9.27×10^{-6} A, respectively), indicating that the two topologies are not meaningfully separated by this metric. Meanwhile, the identified value of $n_3=1.940$ approaches the imposed upper bound of $n_3=2$, suggesting that the optimizer is pushing this parameter against its physical constraint rather than converging to a well-defined interior optimum. This behavior points to limited practical identifiability of the additional TDM parameters under the considered experimental conditions, particularly due to the limited number of irradiance levels and the use of a single temperature. Therefore, the DDM provides a more appropriate balance between model complexity and predictive performance for the investigated PV module, while the TDM is retained for comparison with approaches reported in the literature.

5. Conclusion

A hybrid WOA-FMO metaheuristic framework was developed and validated for parameter extraction of the Solarex MSX60 photovoltaic module under different irradiance conditions. The proposed optimizer integrates Latin Hypercube Sampling combined with Opposition-Based Learning, reflection-based boundary management, adaptive elitism preservation, and dimension-scaled population sizing. Under a consistent benchmarking protocol, WOA-FMO achieved an RMSE of (3.71×10^{-2} A with (R^2>0.998) across the three diode topologies, while outperforming PSO, GA, standard WOA, AOA, and SMA at a comparable computational cost. The statistical analysis further confirmed the significance of these improvements.

A BiLSTM-based residual correction was also evaluated using a leave-one-irradiance-out cross-validation protocol. The results showed that the neural correction did not improve the generalization performance of the physical model, with (λ_{DL}=1) for all considered topologies and validation folds. Consequently, the final model is effectively governed by the WOA-FMO physical formulation. The results also indicate that the DDM provides a favorable balance between accuracy and model complexity, whereas the additional diode in the TDM exhibits limited practical identifiability under the available experimental conditions.

The main limitation of this study is the experimental validation at a single temperature and three irradiance levels. Future work will therefore focus on acquiring verified I-V measurements at multiple temperatures to assess the temperature-dependent formulation, as well as on investigating physics-informed learning approaches that may improve out-of-distribution generalization. The identified physical models will also be considered for implementation on embedded platforms for real-time photovoltaic monitoring and fault diagnosis.

6. References

[1] A. Jain, « Exact analytical solutions of the parameters of real solar cells using Lambert W-function », Sol. Energy Mater. Sol. Cells, vol. 81, no 2, p. 269‑277, févr. 2004, doi: 10.1016/j.solmat.2003.11.018.

[2] T. Easwarakhanthan, J. Bottin, I. Bouhouch, et C. Boutrit, « Nonlinear Minimization Algorithm for Determining the Solar Cell Parameters with Microcomputers », Int. J. Sol. Energy, vol. 4, no 1, p. 1‑12, janv. 1986, doi: 10.1080/01425918608909835.

[3] J. Kennedy et R. Eberhart, « Particle swarm optimization », in Proceedings of ICNN'95 - International Conference on Neural Networks, Perth, WA, Australia: IEEE, 1995, p. 1942‑1948. doi: 10.1109/ICNN.1995.488968.

[4] A. M. Dizqah, A. Maheri, et K. Busawon, « An accurate method for the PV model identification based on a genetic algorithm and the interior-point method », Renew. Energy, vol. 72, p. 212‑222, déc. 2014, doi: 10.1016/j.renene.2014.07.014.

[5] S. Mirjalili et A. Lewis, « The Whale Optimization Algorithm », Adv. Eng. Softw., vol. 95, p. 51‑67, mai 2016, doi: 10.1016/j.advengsoft.2016.01.008.

[6] D. Yousri, S. B. Thanikanti, D. Allam, V. K. Ramachandaramurthy, et M. B. Eteiba, « Fractional chaotic ensemble particle swarm optimizer for identifying the single, double, and three diode photovoltaic models' parameters », Energy, vol. 195, p. 116979, mars 2020, doi: 10.1016/j.energy.2020.116979.

[7] H. M. Ridha, H. Hizam, S. Mirjalili, M. L. Othman, M. E. Ya'acob, et M. Ahmadipour, « Parameter extraction of single, double, and three diodes photovoltaic model based on guaranteed convergence arithmetic optimization algorithm and modified third order Newton Raphson methods », Renew. Sustain. Energy Rev., vol. 162, p. 112436, juill. 2022, doi: 10.1016/j.rser.2022.112436.

[8] S. Hochreiter et J. Schmidhuber, « Long Short-Term Memory », Neural Comput., vol. 9, no 8, p. 1735‑1780, nov. 1997, doi: 10.1162/neco.1997.9.8.1735.

[9] M. Schuster et K. K. Paliwal, « Bidirectional recurrent neural networks », IEEE Trans. Signal Process., vol. 45, no 11, p. 2673‑2681, nov. 1997, doi: 10.1109/78.650093.

[10] H. E. Elwaer, S. A. Avci, et J. Rahebi, « A Fuzzy Fishier Mantis Optimizer method for MPPT in PV solar system », Sci. Rep., vol. 16, no 1, p. 17940, avr. 2026, doi: 10.1038/s41598-026-48694-x.

[11] M. G. Villalva, J. R. Gazoli, et E. R. Filho, « Comprehensive Approach to Modeling and Simulation of Photovoltaic Arrays », IEEE Trans. Power Electron., vol. 24, no 5, p. 1198‑1208, mai 2009, doi: 10.1109/TPEL.2009.2013862.

[12] J. A. Gow et C. D. Manning, « Development of a photovoltaic arraymodel for use in power-electronics simulation studies », IEE Proc. - Electr. Power Appl., vol. 146, no 2, p. 193‑200, mars 1999, doi: 10.1049/ip-epa:19990116.

[13] V. Khanna, B. K. Das, D. Bisht, Vandana, et P. K. Singh, « A three diode model for industrial solar cells and estimation of solar cell parameters using PSO algorithm », Renew. Energy, vol. 78, p. 105‑113, juin 2015, doi: 10.1016/j.renene.2014.12.072.

[14] A. Graves et J. Schmidhuber, « Framewise phoneme classification with bidirectional LSTM and

other neural network architectures », Neural Netw., vol. 18, no 5‑6, p. 602‑610, juill. 2005, doi: 10.1016/j.neunet.2005.06.042.

[15] D. P. Kingma et J. Ba, « Adam: A Method for Stochastic Optimization », 2014, arXiv. doi: 10.48550/ARXIV.1412.6980.

[16] B. P. Singh, S. K. Goyal, et S. A. Siddiqui, « Maximum power point estimation of MSX-60 poly-crystalline standalone solar PV system », Mater. Today Proc., vol. 79, p. 424‑429, 2023, doi: 10.1016/j.matpr.2022.12.268.

[17] L. Abualigah, A. Diabat, S. Mirjalili, M. Abd Elaziz, et A. H. Gandomi, « The Arithmetic Optimization Algorithm », Comput. Methods Appl. Mech. Eng., vol. 376, p. 113609, avr. 2021, doi: 10.1016/j.cma.2020.113609.

[18] S. Li, H. Chen, M. Wang, A. A. Heidari, et S. Mirjalili, « Slime mould algorithm: A new method for stochastic optimization », Future Gener. Comput. Syst., vol. 111, p. 300‑323, oct. 2020, doi: 10.1016/j.future.2020.03.055.

[19] W. H. Kruskal et W. A. Wallis, « Use of Ranks in One-Criterion Variance Analysis », J. Am. Stat. Assoc., vol. 47, no 260, p. 583‑621, déc. 1952, doi: 10.1080/01621459.1952.10483441.

[20] F. Wilcoxon, « Individual Comparisons by Ranking Methods », Biom. Bull., vol. 1, no 6, p. 80, déc. 1945, doi: 10.2307/3001968.